



Electrochemical membrane cell for NH₃ synthesis from N₂ and H₂O by electrolysis at 200 to 250°C using a Ru catalyst, hydrogen-permeable Pd membrane and phosphate-based electrolyte

Journal:	<i>Sustainable Energy & Fuels</i>
Manuscript ID	SE-ART-02-2018-000054.R1
Article Type:	Paper
Date Submitted by the Author:	24-Mar-2018
Complete List of Authors:	Imamura, Kanako; Fukuoka University, Chemical Engineering Kubota, Jun; Fukuoka University, Chemical Engineering



Sustainable Energy & Fuels

Paper

Electrochemical membrane cell for NH₃ synthesis from N₂ and H₂O by electrolysis at 200 to 250°C using a Ru catalyst, hydrogen-permeable Pd membrane and phosphate-based electrolyte

Received 00th January 20xx,
Accepted 00th January 20xx

DOI: 10.1039/x0xx00000x

www.rsc.org/

Kanako Imamura^a and Jun Kubota^{a*}

Ammonia (NH₃) is an energy carrier that can be synthesized from nitrogen and water using electricity generated from renewable sources. The present work investigated NH₃ synthesis using an electrochemical system with the structure of Ru/Cs⁺/MgO|Pd-Ag|CsH₂PO₄/SiP₂O₇|Pt and operating at 200 to 250°C. In this system, the NH₃ being generated is isolated from the CsH₂PO₄/SiP₂O₇ electrolyte by the hydrogen-permeable Pd-Ag membrane, resulting in the production of dry NH₃. A maximum NH₃ synthesis rate of 0.90 nmol s⁻¹ cm⁻² was obtained from the cathode at the Ru/Cs⁺/MgO|Pd-Ag side at a current density of 10 mA cm⁻², temperature of 250°C and N₂ flow rate of 3 cm³ min⁻¹ as converted to standard temperature and pressure. Deviations in the NH₃ production rate from the theoretical amounts predicted by Arrhenius plots were observed at temperatures approaching 250°C, possibly because the reaction approached equilibrium. A current efficiency for NH₃ production of 2.6% was obtained, with the remainder of the current consumed during H₂ generation. The apparent activation energies for the NH₃ synthesis were 69 and 93 kJ mol⁻¹ at 3.2 and 10 mA cm⁻², respectively. These values are significantly lower than that reported for conventional NH₃ synthesis from nitrogen and hydrogen (139 kJ mol⁻¹) over the same catalyst in this cell. The optimum N₂ flow rates were approximately 0.5 and 5 cm³ min⁻¹ at 3.2 and 10 mA cm⁻², respectively, representing nitrogen amounts approximately 42 times the stoichiometric quantities. The provision of an excess of N₂ is believed to reduce the suppression of N₂ activation by so-called hydrogen poisoning of the catalyst.

1. Introduction

Ammonia (NH₃) is one of the most widely used chemical products on a worldwide basis; 170 to 180 million tons of NH₃ are synthesized annually, using atmospheric N₂ and H₂ obtained from fossil fuels, via the so-called Haber-Bosh process.¹⁻³ Over 80% of this NH₃ is currently employed for agricultural fertilization, and is thus of vital importance to society.⁴⁻¹⁴ Recently, it has been demonstrated that NH₃ can be directly used as a fuel in combustion engines¹⁴ and fuel cells¹⁵⁻¹⁸ and that it can be converted to H₂ by catalytic decomposition.^{19,20} The emissions from these systems are ideally only N₂ and H₂O, which is advantageous compared to carbon-based fuels that emit CO₂. The ready liquefaction of NH₃ (which has a boiling point of -33.3°C at 101 kPa and 20°C at 860 kPa) is also an advantage. The mass-based percentage of H₂ in NH₃ is 17.6%, which is much higher than the levels in organic hydrides and hydrogen-storage alloys. In addition, a certain level of infrastructure for the transportation and storage of NH₃ is already in place based on its current usage. Up to now, most hydrogen for the synthesis of NH₃ has been obtained from the conversion of fossil fuels, so that the use of NH₃ as a fuel appears counter-productive. However, if NH₃ can be produced

from N₂ and H₂O using renewable energy and without fossil fuels, it could represent a viable chemical energy carrier. Thus, the synthesis of NH₃ using renewable energies has attracted significant attention as a means of achieving a sustainable energy society.

Even using conventional technologies, NH₃ could conceivably be synthesized by a combination of water electrolysis (based on renewable electricity sources such as wind, solar, and hydro) and the Haber-Bosh process.²¹⁻²³ In fact, hydrogen derived from water electrolysis using hydroelectric energy has already been applied to NH₃ synthesis. The one serious drawback associated with this system is that the Haber-Bosh process is highly exothermic, with a heat of reaction of 91 kJ mol⁻¹.¹⁻³ Therefore, considerable heat is released, and essentially wasted, during NH₃ synthesis. Although water electrolysis is endothermic, the waste heat from NH₃ synthesis cannot readily be employed for the latter process because the two processes are typically physically separated and run at different temperatures. If NH₃ could be synthesized directly from nitrogen and water by electrolysis, this energy loss could be avoided.²⁴⁻²⁷ Furthermore, the direct electrochemical synthesis of NH₃ should be able to proceed in association with small-scale fluctuating electrical power.²⁴⁻²⁷ In fact, both fuel cells and water electrolysis systems can operate in conjunction with dispersed off-grid power systems connected to fluctuating electric power. Therefore, the electrochemical synthesis of NH₃ from nitrogen and water has attracted

^a Department of Chemical Engineering, Fukuoka University, 8-19-1, Nanakuma, Jonan-ku, Fukuoka 814-0180, Japan

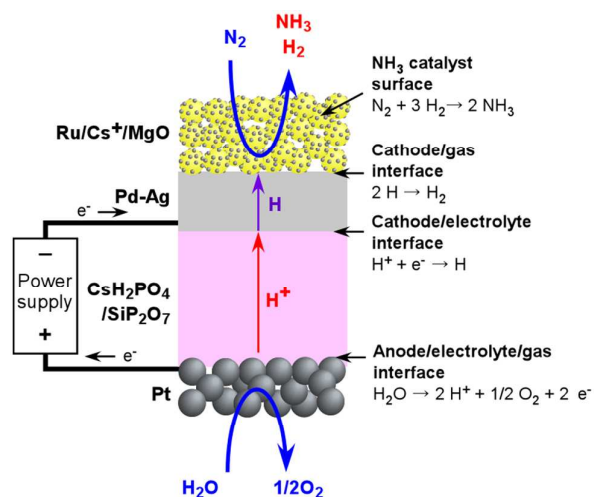


Fig. 1 NH₃ synthesis system employing a Ru/Cs⁺/MgO|Pd-Ag|C₆H₅PO₄/SiP₂O₇|Pt electrochemical cell operating at 200 to 250°C. Chemical reaction equations for respective interfaces are shown in the figure.

significant attention, and there has been much research in this field.²⁴⁻²⁷ An additional advantage of the direct electrochemical synthesis of NH₃ is that the cathodic conditions has possibility to promote the electrochemical activation of N₂ at the electrode interface as explained by the non-faradic electrochemical modification of catalytic activity (NEMCA) effect.^{28,29} However, the presence of NEMCA effect in the nitrogen activation and NH₃ synthesis has been still controversial; some reports propose that NEMCA is negligibly weak,^{28,30} while the other report indicates the presence of electrochemical promotion.³¹

There have been many attempts to develop an electrochemical synthesis of NH₃. Electrolysis using molten salt systems such as LiCl-KCl and LiCl-KCl-CsCl (at 300 and 450°C, respectively) has been applied to the generation of NH₃ from N₂ and H₂O.^{32,33} The electrochemical synthesis of NH₃ using H⁺-conducting solid oxide electrolytes at 500 to 1000°C, has also been intensively studied.^{24-27,34} Based on the reaction equilibrium between NH₃ and N₂/H₂, a low reaction temperature is preferred for NH₃ formation. As such, regardless of the electrochemical potential of the electrode, NH₃ is readily decomposed to N₂ and H₂ over various surfaces at higher temperatures. Electrolysis with phosphate electrolytes over the relatively low temperature range of 180 to 250°C has been examined for this reason.^{35,36} Polymer electrolyte systems operating below 100°C have been also studied by several researchers.^{24-27,37,38} However, although there have been numerous attempts at developing an electrochemical NH₃ synthesis, working at a wide variety of temperatures, a system with a suitable level of efficiency has not yet been developed.²⁴⁻²⁷

As discussed, the electrochemical synthesis of NH₃ involves various challenges. As an example, the reaction going from N₂ and H₂ to NH₃ is exothermic and thus is unfavourable at high temperatures.¹⁻³ For this reason, high temperature electrolysis in the range of 600–1000°C using solid oxide electrolysis cells (SOECs), a range which is much higher than the typical Haber-Bosch temperature span of 400 to 500°C, is not appropriate. At such high temperatures, NH₃ is readily decomposed to N₂ and H₂ even when rapidly generated under electrochemical conditions. In contrast, at relatively low temperatures (below 100°C), the chemical equilibrium favours the formation of NH₃. Polymer electrolyte electrolysis cells (PEECs) can operate in this temperature range, although it is extremely difficult to promote the dissociative adsorption of N₂ on solid-catalyst surfaces (that is, the activation of N₂) at these temperatures.³⁹ It is evident that solid electrolyte systems are helpful when working with a gaseous reactants because the large surface area of the electrocatalysts would not be covered with the liquid electrolyte. On this basis, our own group has focused on the synthesis of NH₃ in the range between 200 and 250°C, in which solid oxoacid compounds may be employed as electrolytes. Among these, phosphates such as C₆H₅(PO₄)₂ and C₆H₅(PO₄)₃ have been intensively studied with regard to applications in fuel cells,⁴⁰⁻⁴⁴ and so were examined in the present work.

Another difficulty associated with the electrochemical synthesis of NH₃ is that the resulting NH₃ is readily exchanged with protons in the proton-conductive electrolyte and thus can be absorbed in various electrolytes, including water, because of the alkaline nature of NH₃ and its affinity for water. Thus, we have proposed the use of hydrogen-permeable alloy membranes at the cathode interface to separate the NH₃ and the acidic electrolyte. Fig. 1 presents a design summarizing the proposed system. The chemical reactions on the respective interfaces are also shown in Fig. 1. Here, hydrogen atoms penetrate the hydrogen-permeable membrane from the cathode/electrolyte interface to the cathode/gas interface, and react with nitrogen on the catalyst surfaces. Since NH₃ synthesis is performed in isolation from the cathode/electrolyte interface, electrochemical effects such as NEMCA cannot be expected for nitrogen activation in this system, in contrast to the pure electrochemical synthesis of NH₃ directly on the cathode catalyst surfaces. It has not been clarified whether the penetrated hydrogen atoms are transferred to NH₃ catalyst surfaces directly with migration on the surfaces or through the gas phase with desorption and adsorption. In the present cell, NH₃ is made without the application of an electrochemical potential, while the electrochemical potential of hydrogen penetrating the hydrogen membrane is controlled by the electrode potential of the hydrogen-permeable membrane.

Our previous communication described a system with the structure of Ru/Cs⁺/MgO|Pd-Ag|C₆H₅PO₄/SiP₂O₇|Pt for the synthesis of NH₃ from N₂ and H₂O at 250°C and 1.2 V, and demonstrated the production of NH₃ in this manner.⁴⁵ However, the limited length of the prior publication precluded a detailed discussion of the associated kinetics and thermodynamics. The experimental techniques and apparatus in the previous work were also primitive in some parts, and have since been

advanced. In this article, the kinetics and thermodynamics of this system are reported and improved NH_3 production is discussed.

2. Experimental section

The electrochemical cell consisted of a $\text{Ru/Cs}^+/\text{MgO}$ catalyst, a Pd-Ag membrane, a $\text{CsH}_2\text{PO}_4/\text{SiP}_2\text{O}_7$ electrolyte and Pt paste. The detail of the materials and experimental procedures are provided in our previous communication and its supporting information.⁴⁵ A catalyst of 2 wt% $\text{Ru/Cs}^+/\text{MgO}$ was prepared by impregnating MgO (Ube Material Industries, Ltd., 500A) with a tetrahydrofuran solution of $\text{Ru}_3(\text{CO})_{12}$ (Furuya Metal Co., Ltd.) with stirring for 8 h at room temperature. The resulting slurry was evaporated using a rotary evaporator below 50°C at reduced pressure. The yellow powder resulting from this step was heated at 300°C under vacuum to decompose the carbonyl groups, then impregnated with an aqueous solution of CsNO_3 (Wako Pure Chemical Industries, Ltd.) at room temperature, and finally dried using a rotary evaporator. The catalyst powder was subsequently heat treated in a tubular furnace at 300°C under a $100\text{ cm}^3_{\text{STP}}\text{ min}^{-1}$ H_2 flow. Here, STP indicates that the volume has been converted to that at standard temperature and pressure (0°C and 101 kPa). The resulting catalyst powder was formed into granules 600–800 μm in size using a hydraulic press.

A Pd-Ag membrane disk, 24 mm in diameter and 0.1 mm thick and containing 25% Ag on a molar basis, was purchased from the Nilaco Co.

The $\text{CsH}_2\text{PO}_4/\text{SiP}_2\text{O}_7$ electrolyte was synthesized by adding the desired amount of H_3PO_4 to an aqueous solution of CsCO_3 , followed by drying of the mixture at 120°C for 24 h. In addition, H_3PO_4 was mixed with SiO_2 and kneaded to obtain a viscous slurry that was subsequently calcined at 200°C for 3 h and 700°C for 3 h. The CsH_2PO_4 and SiP_2O_7 obtained from the above procedures were combined in a 1:2 molar ratio and then crushed and mixed in a mortar. The resulting powder was formed into a disk 20 mm in diameter and 2 mm thick by a hydraulic press.

Pt paste (Tanaka Kikinzoku Kogyo K.K.) was applied to a

20 mm diameter section of carbon paper (Toray, TGP-H-120H) at a density of 3 mg-Pt cm^{-2} . The Pd-Ag membrane, $\text{CsH}_2\text{PO}_4/\text{SiP}_2\text{O}_7$ electrolyte and Pt/carbon paper were then stacked on top of one another and hot-pressed at 3 MPa and 220°C to obtain a membrane-electrolyte-electrode assembly. This assembly, together with 600 mg of the catalyst (191 mg cm^{-2}) was placed in a stainless steel cell equipped with an electric heater and thermocouple. The cell was transferred to an oven and heated at 100°C to avoid condensation of water being supplied through tubes connected to the cell.

A flow of N_2 or N_2+H_2 was sent to the cathode ($\text{Ru/Cs}^+/\text{MgO}$) side of the apparatus using mass flow controllers. The anode (Pt/carbon paper) side was supplied with Ar at $10\text{ cm}^3_{\text{STP}}\text{ min}^{-1}$ using a mass flow controller, with the addition of H_2O at $0.016\text{ cm}^3_{\text{liq}}\text{ min}^{-1}$ via a syringe pump. The gaseous products released from the cathode side were intermittently sampled and analysed using a gas chromatograph with a thermal conductivity detector (GC-TCD, GL Sciences, GC-3200) to estimate the concentration of H_2 . Otherwise, the gases were bubbled through a stirred 25 ml quantity of an aqueous 1 mM H_2SO_4 solution to allow the amount of NH_3 produced to be determined based on decreases in the electrical conductivity of the solution.

Prior to the electrochemical NH_3 synthesis, a N_2+H_2 mixture was passed through the cathode side at 250°C for at least 8 h to reduce the Ru catalyst. After the NH_3 synthesis was observed to achieve equilibrium conditions, the H_2 flow was cut and electrolysis was initiated.

Transmission electron microscopy (TEM) images were obtained using a JEOL JEM-2100F at Kyushu University, Japan and a TEM image of the $\text{Ru/Cs}^+/\text{MgO}$ is shown in Fig. 3. Small black particles with diameters of several nm are evident on MgO particles with sizes of several tens of nm. It is also apparent that the Ru is well dispersed as nm-scale particles on the MgO .

3. Results and discussion

3.1 NH_3 synthesis from N_2 and H_2O

The amounts of NH_3 formed over time at various

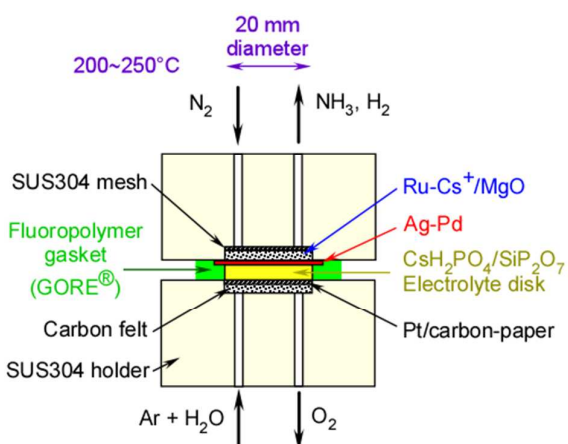


Fig. 2 Diagram of the $\text{Ru/Cs}^+/\text{MgO}|\text{Pd-Ag}|\text{CsH}_2\text{PO}_4/\text{SiP}_2\text{O}_7|\text{Pt}$ cell for NH_3 synthesis from N_2 and H_2O via electrolysis.

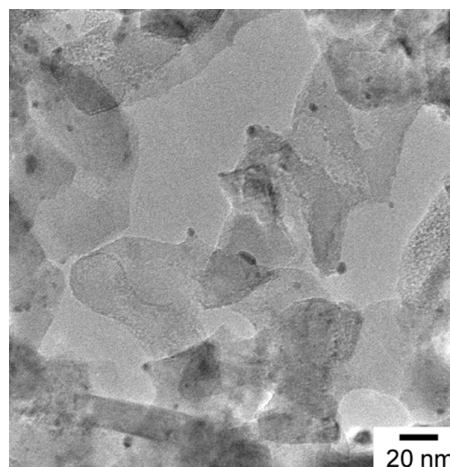


Fig. 3 TEM image of $\text{Ru/Cs}^+/\text{MgO}$ catalyst, which was located over the Pd-Ag membrane in the cell.

ARTICLE

Sustainable Energy & Fuels

temperatures are summarized in Fig. 4. The quantities of NH_3 obtained in each trial were determined from changes in the electro-conductivity of the 1 mM H_2SO_4 solution that absorbed the gases exiting the cell. NH_3 formation is seen to increase monotonically over time in each case, such that the rates of formation at each temperature could be estimated from the slopes. During these trials, the cell was operated at a constant current of 10 mA cm^{-2} and the N_2 flow to the cathode was $3 \text{ cm}^3_{\text{STP}} \text{ min}^{-1}$. The highest NH_3 formation rate of $0.90 \text{ nmol s}^{-1} \text{ cm}^{-2}$ was obtained at 250°C . The 2 wt%-Ru/Cs⁺/MgO catalyst loading of 191 mg cm^{-2} corresponds to a mass-based reaction rate of $17.0 \text{ } \mu\text{mol h}^{-1} \text{ g}^{-1}$. Previously, a NH_3 synthesis rate over a 2 wt%-Ru/Cs⁺/MgO catalyst of approximately 1 mmol g^{-1} was reported at 315°C and 101 kPa.^{45,46} Assuming that the apparent activation energy for NH_3 synthesis is 139 kJ mol^{-1} in this temperature region (see the subsequent discussion), the NH_3 generation rate at 315°C should be 35 times that at 250°C , and so the value of $17.0 \text{ } \mu\text{mol h}^{-1} \text{ g}^{-1}$ obtained in this work is reasonable. As outlined further on, the rate of NH_3 formation was limited by the chemical equilibrium of the synthesis reaction, such that the rate was less than the theoretical value.

The NH_3 formation rates at current densities of 3.2 and 10 mA cm^{-2} are shown as Arrhenius plots in Fig. 5, along with the rates obtained from a mixture of N_2 and H_2 in the present cell without electrolysis. It is evident that the absolute rates of NH_3 formation at both current densities were much higher than that for catalytic NH_3 formation from the mixture of N_2 and H_2 below 230°C , even when the N_2 and H_2 flows were higher than that for the electrolysis. It should also be noted that the current density of 10 mA cm^{-2} was equivalent to a H_2 flow of only $0.22 \text{ cm}^3_{\text{STP}} \text{ min}^{-1}$. The apparent activation energy values for NH_3 formation using electrolysis at 3.2 and 10 mA cm^{-2} were estimated to be 69 and 93 kJ mol^{-1} , respectively. In contrast, the apparent activation energy for NH_3 formation from N_2 and H_2

was 139 kJ mol^{-1} , which is slightly higher than previously reported values, possibly because of the relatively low temperature compared to those typically applied for NH_3 synthesis (300 to 500°C).^{45,46} It may also be that adsorbed intermediate species behaved as inhibitors to increase the apparent activation energy. Since the apparent activation energy for NH_3 formation via electrolysis was not far from that for a more typical NH_3 synthesis, the rate determining process in the present system is believed to be the dissociative adsorption of N_2 on the Ru/Cs⁺/MgO catalyst, just as in a standard NH_3 synthesis.^{1,46,47}

It should be noted that the apparent activation energy for NH_3 synthesis via electrolysis was lower than that for synthesis from a mixture of N_2 and H_2 without electrolysis. In addition, the absolute rates of NH_3 formation with electrolysis were higher than those without the electrolysis. The H_2 transport rates from the Pd-Ag membrane to the Ru catalyst side were

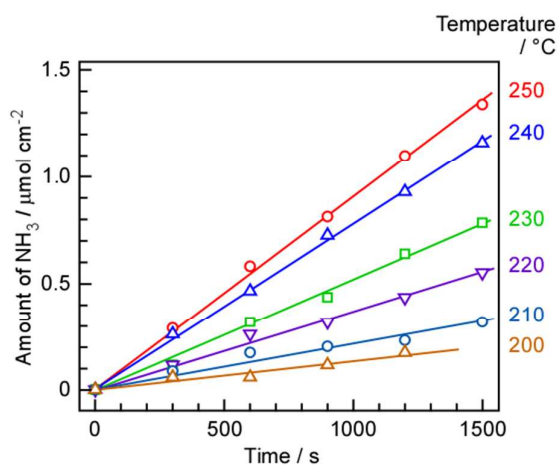


Fig. 4 Time courses of NH_3 formation at various temperatures and 10 mA cm^{-2} , using N_2 as the cathode gas at $3 \text{ cm}^3_{\text{STP}} \text{ min}^{-1}$.

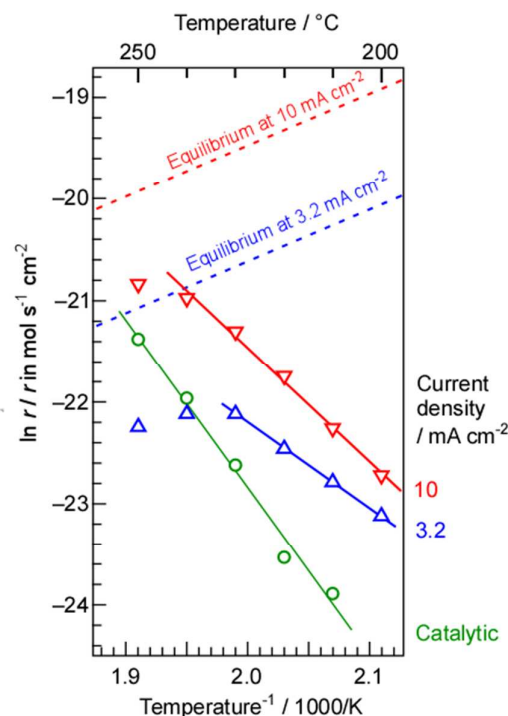


Fig. 5 Arrhenius plots of NH_3 synthesis rates at current densities of 3.2 and 10 mA cm^{-2} and N_2 flow rates to the cathode of 1 and $3 \text{ cm}^3_{\text{STP}} \text{ min}^{-1}$, respectively. The NH_3 synthesis rates with flows of H_2 ($30 \text{ cm}^3_{\text{STP}} \text{ min}^{-1}$) and N_2 ($10 \text{ cm}^3_{\text{STP}} \text{ min}^{-1}$) to the cathode side without electrolysis are also shown for comparison purposes. The dashed lines indicate the limit of NH_3 synthesis rates by the chemical equilibrium for 3.2 and 10 mA cm^{-2} .

estimated to be 17 and $52 \text{ nmol s}^{-1} \text{ cm}^{-2}$ based on current densities of 3.2 and 10 mA cm^{-2} , respectively, N_2 flow rates of 1 and $3 \text{ cm}^3_{\text{STP}} \text{ min}^{-1}$ are equivalent to 240 and

710 nmol s⁻¹ cm⁻². Therefore, the amount of N₂ provided to the Ru catalyst was approximately 42 times (H₂/N₂=0.071) the stoichiometric quantity (H₂/N₂=3) based on the amount of H₂. As demonstrated in the following section, this flow rate was almost optimum for the applied current density. Ru-based NH₃ catalysts are known to undergo so-called hydrogen poisoning, such that the reaction order for NH₃ synthesis with respect to H₂ pressure is typically negative (-1.0 to -0.1, except for a few rare cases).⁴⁶ In the case of Ru catalysts, hydrogen covers the Ru surfaces to block the dissociative adsorption of N₂. Therefore, we conclude that the lower apparent activation energy for NH₃ synthesis with electrolysis resulted from the excess N₂ flow. The dependence of the rate of NH₃ formation on the N₂ flow rate is examined in Section 3.2.

Another important aspect of the Arrhenius plots is the deviation from the theoretical slope at relatively high temperatures. Because NH₃ synthesis is exothermic, the chemical equilibrium can limit the reaction rate at high temperatures. The thermodynamic limits by the chemical equilibrium of NH₃ with N₂ flow and H₂ from the electrolysis were estimated against the present H₂/N₂ ratio at respective temperatures as discussed in section 3.3, and those are also shown in Fig. 5 by dashed lines. Evidently, the rates of NH₃ formation were approaching to the equilibrium limits shown by the dashed lines around 250°C. Thus, this deviation from the Arrhenius slope around 250°C can be reasonably explained from that the reaction is approaching equilibrium.

The NH₃ formation rates and current efficiencies for NH₃ and H₂ are summarized in Table 1. Current efficiency, also known as Faradaic efficiency (*FE*), is defined as²⁴⁻²⁷

$$FE = \frac{3 \times N}{F \times Q} \times 100 \quad ,$$

where *N*, *F* and *Q* are the amount of NH₃ generated (mol), the Faraday constant (96500 C mol⁻¹) and the electric charge through the cell (C), respectively. The Faraday reaction in the present system involved only the reduction of protons to hydrogen atoms, such that NH₃ was produced without any charge transfer reaction. Therefore, in this paper, the *FE* indicates the total current efficiency associated with the production of NH₃ and H₂ in the cell. That is, it is the ratio of the actual to the ideal amounts of H₂ electrolyzed to NH₃. The theoretical thermodynamic equilibrium was calculated as described in section 3.3. The degree of attainment of equilibrium (%), *AE*, for NH₃ formation was estimated as listed in Table 1. At 10 mA cm⁻², 3 cm³_{STP} min⁻¹ and 250°C, approximately 2.6% of the current was used for NH₃ formation, while the remaining part was employed for H₂ formation (based on GC analysis). It should be noted that an experimental error of about ±5% was associated with the estimated rates of formation of NH₃ and H₂ in this work. The sum of the current efficiencies for NH₃ and H₂ was almost 100% above 220°C. It is therefore evident that detrimental processes, such as the emission of H₂ from the Pd-Ag membrane to the anode side and leakage of O₂ around the anode to the Pd-Ag side through the electrolyte, occurred to a minimal extent. At 10 mA cm⁻², the sum of the current efficiencies was slightly below 100% at 200-210°C. It is possible that the H₂ and O₂ products underwent cross-over in the cell to reduce the current efficiency. The current efficiencies sum was also less than 100% at 0.5-1.0 cm³_{STP} min⁻¹ and 3.2 mA cm⁻², due to the experimental error in accurately setting the N₂ flow rate via the mass flow controller at low flows. The concentration of H₂ in the product gas was based on the amount of N₂, so that any error in the N₂ flow rate was directly reflected in the estimated rate of H₂ formation.

Table 1 NH₃ formation rates and current efficiencies at various current densities, N₂ flow rates and temperatures.

Current mA cm ⁻²	N ₂ Flow ^{a)} cm ³ min ⁻¹	Temp. °C	<i>r</i> _{NH₃} ^{b)} nmol s ⁻¹ cm ⁻²	<i>FE</i> _{NH₃} ^{c)} %	<i>AE</i> ^{d)} %	<i>FE</i> _{H₂} ^{e)} %
10	3.0	200	0.14	0.39	2.2	85
		210	0.22	0.62	4.3	95
		220	0.37	1.1	9.4	100
		230	0.52	1.5	16	101
		240	0.78	2.3	29	102
		250	0.90	2.6	41	103
3.2	0.5	250	0.17	1.5	24	65
	1.0	250	0.28	2.5	40	82
	2.0	250	0.27	2.5	38	95
	5.0	250	0.18	1.6	25	103
	7.0	250	0.15	1.4	21	100

a) Flow rates are in standard temperature and pressure, cm³_{STP} min⁻¹

b) Rate of NH₃ formation.

c) Current efficiency for NH₃ formation.

d) Degree of attainment of thermodynamic equilibrium

e) Current efficiency for H₂ formation.

3.2 Dependence on the flow rate of N₂

As discussed in Section 3.1, the optimal N₂ flow rate greatly exceeded the stoichiometric requirement based on the amount of H₂. Thus, it is possible that lowering the N₂ flow rate may increase the rate of NH₃ formation. In fact, our previous work indicated that the rate of NH₃ formation was increased upon decreasing the N₂ flow rate, and so the N₂ flow rate to the Ru/Cs⁺/MgO side was varied to investigate the kinetics of the present system. The results are shown in Fig. 6, and demonstrate that the maximum NH₃ formation rates were 0.5 to 1.0 and 5 to 7 cm³_{STP} min⁻¹ at current densities of 3.2 and 10 mA cm⁻², respectively. As discussed in Section 3.1, the N₂ flow rate was 42 times higher (H₂/N₂=0.071) than the stoichiometric requirement at 1.0 cm³_{STP} min⁻¹ and 3.2 mA cm⁻². This ratio However, the maximum rate of NH₃ formation was obtained at a similarly unbalanced ratio of N₂ and H₂. Based on chemical equilibrium, the stoichiometric ratio of N₂ to H₂ should provide the highest rate of NH₃ formation, as discussed in Section 3.3. This is in agreement with our previous observation that the NH₃ production rate was

ARTICLE

Sustainable Energy & Fuels

increased when reducing the N_2 flow rate over the range between 1 to $7 \text{ cm}^3_{\text{STP}} \text{ min}^{-1}$ at 3.2 mA cm^{-2} .

There are two possible reasons why the NH_3 formation was reduced along with the N_2 flow rate in the present study. The most likely cause is that NH_3 synthesis on the Ru catalyst was greatly suppressed by increases in the proportion of H_2 . That is, hydrogen poisoning of the catalyst decreased the rate of NH_3 formation at lower N_2 flow rates, meaning that an excess of N_2 is required to avoid this effect. The other possibility is that this cell operated under very complex conditions. In this apparatus, NH_3 is synthesized on the catalyst layer under a counter-flow of N_2 and H_2 , but there is no evidence that the N_2 and H_2 undergo typical counter-flow diffusion. It may be that local flow channels are formed in the catalyst layer and various hydrodynamic effects become important. Although the latter effect should be considered, it is thought that the decreased synthesis rate at lower N_2 flows resulted primarily from hydrogen poisoning.

3.3 Chemical equilibrium of NH_3 synthesis

The Arrhenius plots in Fig. 5 suggest that the rate of NH_3 formation was close to that expected from the chemical equilibrium among N_2 , H_2 and NH_3 at 250°C . Fig. 7 plots the theoretical NH_3 partial pressures at 250°C and a total pressure of 101.3 kPa as calculated using 46.1 kJ mol^{-1} as the heat of formation for NH_3 (ΔH_f°) and $-16.5 \text{ kJ mol}^{-1}$ as the Gibbs energy change for the reaction (ΔG_r°). The temperature-dependent molar specific heats at constant pressure used in these calculation were⁴⁸

$$\begin{aligned} N_2: & 28.9 - 1.57 \times 10^{-3} T + 8.08 \times 10^{-6} T^2 - 2.87 \times 10^{-9} T^3 \text{ (J mol}^{-1} \text{ K}^{-1}), \\ H_2: & 29.1 - 1.92 \times 10^{-3} T + 4.00 \times 10^{-6} T^2 - 8.70 \times 10^{-10} T^3 \text{ (J mol}^{-1} \text{ K}^{-1}), \\ NH_3: & 27.6 + 2.56 \times 10^{-2} T + 9.91 \times 10^{-6} T^2 - 6.69 \times 10^{-9} T^3 \text{ (J mol}^{-1} \text{ K}^{-1}), \end{aligned}$$

where T is the absolute temperature. The conversion for H_2

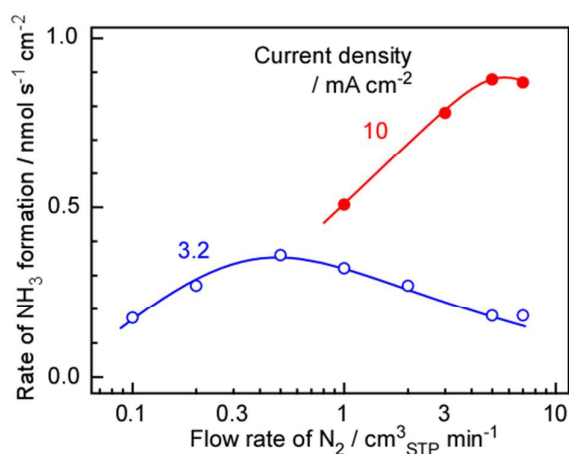


Fig. 6 Rate of NH_3 formation as a function of the flow rate of N_2 at 250°C and current densities of 3.2 (filled circles) and 10 mA cm^{-2} (solid circles).

($\text{Conv}(H_2)$) is equivalent to the FE for NH_3 formation and the remaining is FE for H_2 formation in the present system. Theoretically, the ratio of FE for NH_3 and H_2 cannot be exceeded over $\text{Conv}(H_2)$ in Fig. 7. At 250°C and a total pressure of 101.3 kPa, a stoichiometric combination of N_2 and H_2 (1:3) will generate 5.1 kPa of NH_3 , where 10% of the N_2 and 10% of the H_2 are converted to NH_3 . However, as discussed above, a 42-fold excess of N_2 was supplied to the cell, such that the H_2/N_2 ratio was 0.071. At this ratio, only 0.27 kPa of NH_3 and 6.4% H_2 conversion would be expected. Thus, FE of 6.4 and 93.6% for NH_3 and H_2 formation are thermodynamic limits in this H_2/N_2 ratio at 250°C . The current efficiency for NH_3 formation obtained during this trial was 2.6%, which is close to half the equilibrium limitation. Therefore, the deviations seen in the Arrhenius plots at high temperature can be reasonably considered to be due to the effects of chemical equilibrium. To obtain the degree of attainment of thermodynamic equilibrium in Table 1, the equilibrium limits in the range between $200\text{--}250^\circ\text{C}$ were similarly estimated. At 200°C , the thermodynamic limit was estimated as 18% in this H_2/N_2 ratio, indicating that the lower temperature is preferable for higher NH_3 production in the view point of chemical equilibrium.

These results suggest that further improvements in the NH_3 formation rate could be obtained by employing a H_2/N_2 ratio closer to the stoichiometric value at $H_2/N_2=3$. Despite this, the optimal N_2 flow rate in Fig. 6 is far from the stoichiometric ratio and the development of catalysts which have optimized for H_2/N_2 ratio of stoichiometry is required. The development of catalysts that are resistant to hydrogen poisoning will therefore be required to realize further improvements.

During the electrochemical synthesis of NH_3 , the limitations

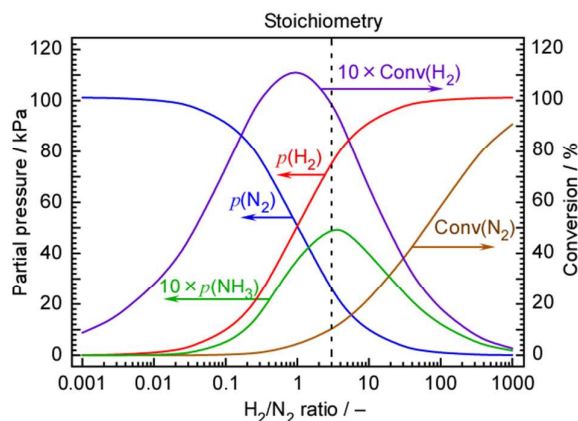


Fig. 7 Partial pressures of various species at chemical equilibrium during NH_3 synthesis as a function of the initial H_2/N_2 ratio at a total pressure of 101 kPa and 250°C . Partial pressures of N_2 , $p(N_2)$, H_2 , $p(H_2)$ and NH_3 , $p(NH_3)$ in equilibrium, and conversions of N_2 , $\text{Conv}(N_2)$ and H_2 , $\text{Conv}(H_2)$, are plotted. Note that both $p(NH_3)$ and $\text{Conv}(H_2)$ are multiplied by 10 in these plots.

imposed by chemical equilibrium are evidently important, because NH_3 is readily decomposed to N_2 and H_2 even if a

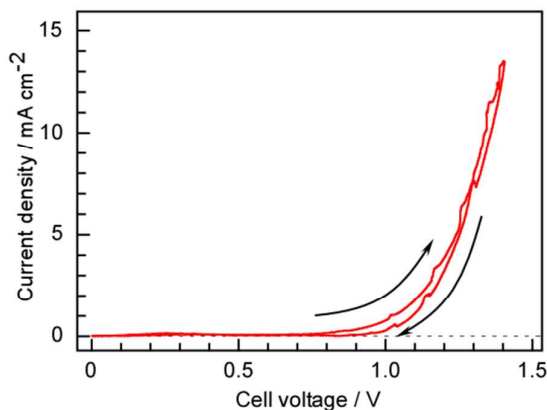


Fig. 8 Cyclic current-voltage profile obtained from the present NH_3 synthesis cell between 0 and -1.4 V at a cell temperature of 250°C, a sweep rate of 0.2 mV s^{-1} and using N_2 as the cathode gas at $3 \text{ cm}^3_{\text{STP}} \text{ min}^{-1}$.

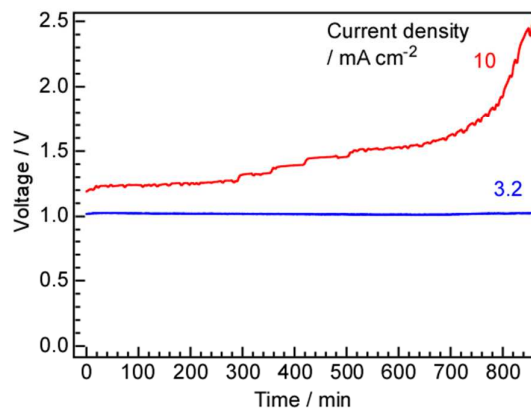


Fig. 9 Time courses of the cell voltage at current density values of 3.2 and 10 mA cm^{-2} at 250°C using N_2 as the cathode gas at $3 \text{ cm}^3_{\text{STP}} \text{ min}^{-1}$.

greater quantity of NH_3 is electrochemically synthesized by a potential effect.

3.4 Current-voltage properties

The current-voltage characteristics of the present cell having a $\text{Ru/Cs}^+/\text{MgO}|\text{Pd-Ag}|\text{CsH}_2\text{PO}_4/\text{SiP}_2\text{O}_7|\text{Pt}$ structure were ascertained via voltage cycling between 0 and 1.4 V at a sweep rate of 0.2 mV s^{-1} . Here, the voltage was defined as the anode potential against the cathode potential. A current appeared around 0.8 V, which is much lower than the theoretical value of 1.15 V for water electrolysis at 250°C under standard pressure conditions. The partial pressure of H_2 in the Ru catalyst layer was far below 101 kPa due to the excess flow of N_2 . Produced O_2 in the anode side was also purged by Ar resulting in the small partial pressure of O_2 . Because, H_2 at the cathode surface and O_2 at the anode surface were purged by N_2 and Ar reducing the partial pressures of H_2 and O_2 , respectively, the practical cell voltage for water electrolysis to form H_2 and O_2 became lower than the theoretical value for the standard pressure. The current was exponentially increased with increasing voltage, indicating that the current was determined by electrochemical reaction kinetics in accordance with the Tafel equation.

3.5 Time courses of the cell voltage

The cell voltage values obtained over time during constant current operation are plotted in Fig. 8. At 3.2 mA cm^{-1} , the voltage was constant at 1.03 V for longer than 800 min, in agreement with behaviour observed in our previous work. In fact, the voltage was found to remain stable over several days, with intermittent starts and stops, when the cell was operated at approximately 3.2 mA cm^{-1} . However, at 10 mA cm^{-1} , the cell voltage increased with time and this increase was exponential after 600 min. This result demonstrates that some components

of the cell were degraded at the higher current density. At present, the cause of this degradation is unclear and additional research is needed to improve the component materials, such as the Ru catalyst, Pd-Ag membrane, electrolyte and anode, as well as to optimize the auxiliary parts, such as the electric conductors, inner cell walls and gaskets.

3.6 General discussion

This work examined the applicability of a $\text{Ru/Cs}^+/\text{MgO}|\text{Pd-Ag}|\text{CsH}_2\text{PO}_4/\text{SiP}_2\text{O}_7|\text{Pt}$ cell to NH_3 synthesis from N_2 and H_2O . It was found that the rate of NH_3 formation was limited by chemical equilibrium. The present FE of NH_3 formation was 2.6% but the equilibrium limit of NH_3 formation was 6.4% of H_2 conversion. To improve the rate of NH_3 formation, lowering temperature of cell can be generally considered. The equilibrium limit of NH_3 formation increases with decreasing temperature because of the exothermic reaction of NH_3 synthesis. However, the activity of present catalyst was not enough to achieve equilibrium especially around 200°C. The development of more active catalysts is required for further improvement of cell. More active catalysts can also reduce the thickness of catalyst layer. The present cell has the thickness of catalyst layer of ca. 2 mm, but that below a few hundred μm is more preferable for the variety of designs of electrochemical cells.

A H_2/N_2 ratio close to the stoichiometric value is expected to give a higher rate of NH_3 formation in the view point of chemical equilibrium. However, the $\text{Ru/Cs}^+/\text{MgO}$ catalyst is prone to hydrogen poisoning and so decreasing the N_2 flow does not enhance NH_3 generation. Thus, limiting the hydrogen poisoning of the Ru catalyst might be the next challenge. Recently, several newer NH_3 catalysts has been proposed, some of which have been reported to exhibit minimal hydrogen poisoning.⁴⁹⁻⁵¹ As an example, the addition of lanthanide

ARTICLE

Sustainable Energy & Fuels

compounds to Ru catalysts has been found to reduce this effect.^{51,52} At present, hydrogen poisoning is the most viable explanation for the need to provide an unbalanced H₂/N₂ ratio to maximize the rate of NH₃ formation.

One advantage of this cell is that the water electrolysis and NH₃ synthesis components are thermally equilibrated in a single unit, resulting in thermodynamics equivalent to those for the pure electrochemical synthesis of NH₃. As such, the exothermic and endothermic NH₃ synthesis and water electrolysis processes balance out, leading to a highly efficient device without appreciable heat loss, just as in the pure electrochemical synthesis of NH₃. Among the elemental steps that occur during the electrochemical synthesis of NH₃, including the reduction of H⁺ to H(ads) (where “ads” refers to an adsorbed species), the activation of N₂ to form N(ads) and the hydrogenation of N(ads) by H(ads) to give NH(ads), NH₂(ads) and NH₃(ads), the sole Faradaic process is the first. It remains uncertain whether or not the application of an electrochemical potential activates N₂ to produce N(ads) or promotes the hydrogenation of N(ads) by H(ads), but these elemental steps are not Faradaic reactions involving charge transfer. In this sense, the present system can be regarded as comparable to the electrochemical synthesis of NH₃. Furthermore, because of the isolation of the NH₃ formation catalyst from the electrode interface by the hydrogen membrane, the NH₃ product is not contaminated with the water that is required for water electrolysis. In addition, the poisoning of the catalyst by humidity is not an issue in the present system.

Proton-conductive polymer membrane electrolytes could also potentially be used in this cell in place of phosphate electrolytes, as the former have already found practical applications in water electrolysis. If the operating temperature could be reduced to approximately 100°C, these polymer membranes could become feasible. Non-precious metal hydrogen-permeable membranes also have potential in the present system.^{53,54} In fact, hydrogen-membrane fuel cells have been proposed,⁵⁵⁻⁵⁷ and show promise as electrochemical systems. At present, we have not successfully applied alternative catalysts, hydrogen-permeable membranes or electrolytes, but these are all still possibilities. Thus, since the selection of materials for use in this work was limited and there is room to improve the system, it is thought that the fusion of technological improvements in catalysis, hydrogen-permeable membranes, and proton-conductive electrolytes will lead to further evolution of this system.

Conclusions

NH₃ synthesis using a Ru/Cs⁺/MgO|Pd-Ag|CsH₂PO₄/SiP₂O₇|Pt cell was investigated in the temperature region between 200 and 250°C. The temperature dependence of the NH₃ formation rate indicated that the rate was influenced by the chemical equilibrium that occurs at high temperatures. The apparent activation energies of the present system were estimated to be 69 and 93 kJ mol⁻¹ at 3.2 and 10 mA cm⁻², respectively, both of which are significantly lower than that for conventional NH₃ synthesis from N₂ + H₂ (139 kJ mol⁻¹). The current efficiency

for NH₃ formation was estimated to be 2.6%, with the remaining current going to H₂ formation. The optimum N₂ flow rates for NH₃ formation were 0.5 to 1.0 and 5 to 7 cm³_{STP} min⁻¹ at current densities of 3.2 and 10 mA cm⁻², respectively, both of which are significantly greater than the stoichiometric amounts. The cell was operated in a stable manner for longer than 800 min at 1.03 V and 3.2 mA cm⁻², although performance degradation within 800 min was observed at 10 mA cm⁻².

Conflicts of interest

The authors declare no conflict of interest.

Acknowledgements

This work was supported as a project under the “Creation of Innovative Core Technology for Manufacture and Use of Energy Carriers from Renewable Energy” CREST program of the Japan Science and Technology Agency (JST).

Note and references

- 1 A. Ozaki, K. Aika, *Catalysis-Science and Technology* Vol 1. (Eds.: J.R. Anderson, M. Boudart), Springer-Verlag KG, Berlin, 1981, pp. 87-158.
- 2 Ammonia: Catalysis and Manufacture, A. Nielsen Ed., Springer-Verlag, Berlin Heidelberg, 1995.
- 3 H. Liu, *Ammonia Synthesis Catalysts: Innovation and Practice*, World Scientific, Singapore, 2013.
- 4 L. Green Jr., *Int. J. Hydrogen Energy*, 1982, **7**, 355-359.
- 5 W.H. Avery, *Int. J. Hydrogen Energy*, 1988, **13**, 761-773.
- 6 C.H. Christensen, T. Johannessen, R.Z. Sørensen, J.K. Nørskov, *Catal. Today*, 2006, **111**, 140-144.
- 7 C. Zamfirescu, I. Dincer, *J. Power Sources*, 2008, **185**, 459-465.
- 8 C. Zamfirescu, I. Dincer, *Fuel Process. Tech.*, 2009, **90**, 729-737.
- 9 F. Schüth, *Chem. Ingen. Tech.* 2011, **83**, 1984-1993.
- 10 R. Lan, J.T.S. Irvine, S. Tao, *Int. J. Hydrogen Energy*, 2012, **37**, 1482-1494.
- 11 D. Miura, T. Tezuka, *Energy*, 2014, **68**, 428-436.
- 12 S. Giddey, S.P.S. Badwal, C. Munnings, M. Dolan, *ACS Sustainable Chem. Eng.*, 2017, **5**, 10231-10239.
- 13 O. Elishav, G. Tvil, B. Mosevitzky, D. Lewin, G.E. Shter, G.S. Grader, *Energy Procedia*, 2017, **135**, 3-13.
- 14 A.J. Reiter, S.-C. Kong, *Fuel*, 2011, **90**, 87-97.
- 15 N.V. Ress, R.G. Compton, *Energy Environ. Sci.*, 2011, **4**, 1255-1260.
- 16 F. Ishak, I. Dincer, C. Zamfirescu, *J. Power Sources*, 2012, **202**, 157-165.
- 17 G. Cinti, U. Desideri, D. Penchini, G. Discepoli, *Fuel Cells*, 2014, **14**, 221-230.
- 18 A.F.S. Molouk, T. Okanishi, H. Muroyama, T. Matsui, K. Eguchi, *J. Electrochem. Soc.*, 2015, **162**, F1268-F1274.
- 19 F. Schüth, R. Palkovits, R. Schlögl, D.S. Su, *Energy Environ. Sci.*, 2012, **5**, 6278-6289.
- 20 K. Sato, N. Abe, T. Kawagoe, S. Miyahara, K. Honda, K. Nagaoka, *Int. J. Hydrogen Energy*, 2017, **42**, 6610-6617.
- 21 T. Grundt, K. Christiansen, *Int. J. Hydrogen Energy*, 1982, **7**, 247-257.
- 22 E. Morgan, J. Manwell, J. McGowan, *Renewable Energy*, 2014, **72**, 51-61.

- 23 J. Tallaksen, F. Bauer, C. Hulteberg, M. Reese, S. Ahlgren, *J. Cleaner Product.*, 2015, **107**, 626-635.
- 24 I.A. Amar, R. Lan, C.T.G. Petit, S. Tao, *J. Solid State Electrochem.*, 2011, **15**, 1845-1860.
- 25 S. Giddey, S.P.S. Badwal, A. Kulkarni, *Int. J. Hydrogen Energy*, 2013, **38**, 14576-14594.
- 26 V. Kyriakou, I. Garagounis, E. Vasileiou, A. Vourros, M. Stoukides, *Catal. Today*, 2017, **286**, 2-13.
- 27 X. Guo, Y. Zhu, T. Ma, *J. Energy Chem.*, 2017, **26**, 1107-1136.
- 28 C. G. Vayenas, S. Bebelis, S. Neophytides, *J. Phys. Chem.*, 1988, **92**, 5083-5085.
- 29 A. Katsaounis, *J. Appl. Electrochem.* 2010, **40**, 885-902.
- 30 I. Garagounis, V. Kyriakou, M. Stoukides, *Solid State Ionics*, 2013, **231**, 58-62.
- 31 F. Kosaka, T. Nakamura, A. Oikawa, J. Otomo, *ACS Sustainable Chem. Eng.* 2017, **5**, 10439-10446.
- 32 T. Murakami, T. Nohira, T. Goto, Y.H. Ogata, Y. Ito, *Electrochim. Acta*, 2005, **50**, 5423-5426.
- 33 Y. Ito, T. Nishikiori, H. Tsujimura, *Faraday Discuss.*, 2016, **190**, 307-326.
- 34 F. Kosaka, N. Noda, T. Nakamura, J. Otomo, *J. Mater. Sci.*, 2017, **52**, 2825-2835.
- 35 G. Qing, R. Kikuchi, S. Kishira, A. Takagaki, T. Sugawara, S.T. Oyama, *J. Electrochem. Soc.*, 2016, **163**, E282-E287.
- 36 G. Qing, K. Sukegawa, R. Kikuchi, A. Takagaki, S.T. Oyama, *J. Appl. Electrochem.*, 2017, **47**, 803-814.
- 37 V. Kordali, G. Kyriacou, Ch. Lambrou, *Chem. Commun.*, 2000, 1673-1674.
- 38 S. Chen, S. Perathoner, C. Ampelli, C. Mebrahtu, D.Su, G. Centi, *Angew. Chem. Int. Ed.*, 2017, **56**, 2699-2703.
- 39 K. Aika, *Angew. Chem. Int. Ed.*, 1986, **25**, 558-559.
- 40 T. Matsui, T. Kukino, R. Kikuchi, K. Eguchi, *J. Electro-chem. Soc.*, 2006, **153**, A339-A342.
- 41 A.B. Papandrew, C.R.I. Chisholm, R.A. Elgammal, M.M. Özer, S.K. Zecevic, *Chem. Mater.*, 2011, **23**, 1659-1667.
- 42 J. Otomo, T. Ishigooka, T. Kitano, H. Takahashi, H. Nagamoto, *Electrochim. Acta*, 2008, **53**, 8186-8195.
- 43 N. Mohammad, A.B. Mohamad, A.A.H. Kadhum, K.S. Loh, *J. Power Sources*, 2016, **322**, 77-92.
- 44 G. Qing, R. Kikuchi, A. Takagaki, T. Sugawara, S.T. Oyama, *J. Power Sources*, 2014, **272**, 1018-1029.
- 45 K. Imamura, M. Matsuyama, J. Kubota, *Chem. Select*, 2017, **2**, 11100-11103.
- 46 K. Aika, *Catal. Today*, 2017, **286**, 14-20.
- 47 K. Aika, T. Takano, S. Murata, *J. Catal.*, 1992, **136**, 126-140.
- 48 O.A. Hougen, K.M. Watson, R.A. Ragatz, *Chemical Process Principles, Part II*, 2nd ed., John Wiley & Sons, New York, 1959.
- 49 M. Kitano, Y. Inoue, Y. Yamazaki, F. Hayashi, S. Kanbara, A. Matsuishi, T. Yokoyama, S. W. Kim, M. Hara, H. Hosono, *Nature Chem.*, 2012, **4**, 934-940.
- 50 M. Hara, M. Kitano, H. Hosono, *ACS Catal.*, 2017, **7**, 2313-2314.
- 51 K. Sato, K. Imamura, Y. Kawano, S. Miyahara, T. Yamamoto, S. Matsumura, K. Nagaoka, *Chem. Sci.*, 2017, **8**, 674.
- 52 Y. Kadowaki, K. Aika, *J. Catal.*, 1996, **161**, 178-185.
- 53 J.N. Armor, *Catal. Today*, 1995, **25**, 199-207.
- 54 C. Kura, Y. Kunisada, E. Tsuji, S. Zhu, H. Habazaki, S. Nagata, T. P. Michael, R. A. de Souza, Y. Aoki, *Nature Energy*, 2017, **2**, 786-794.
- 55 Y. Aoki, S. Kobayashi, T. Yamaguchi, E. Tsuji, H. Habazaki, K. Yashiro, T. Kawada, T. Ohtsuka, *J. Phys. Chem. C*, 2016, **120**, 15976-15985.
- 56 N. Ito, M. Iijima, K. Kimura, S. Iguchi, *J. Power Source*, 2005, **152**, 200-203.
- 57 N. Ito, S. Aoyama, T. Masui, S. Matsumoto, H. Matsumoto, T. Ishihara, *J. Power Sources*, 2008, **185**, 922-926.

Graphical Abstract

An electrochemical membrane cell for NH_3 synthesis from N_2 and H_2O by electrolysis at 200 to 250°C using a Ru catalyst, hydrogen-permeable Pd membrane and phosphate-based electrolyte

Kinetic properties of NH_3 synthesis from N_2 and H_2O by electrolysis using a combination of a Ru/Cs⁺/MgO catalyst, a Pd-Ag membrane, a CsH₂PO₄/SiP₂O₇ electrolyte and a Pt electrode are investigated.

Kanako Imamura^a and Jun Kubota^{a*}

Simple electrochemical device for NH_3 production

